JVC

Journal of Vibration and Control
000(00) 1–14

DOI: 10.1177/1077546310362451
jvc.sagepub.com
SAGE

Preview Control of Slow-active Suspension Systems

M M ElMadany[1], B A Al Bassam[1] and A A Fayed[2]

Abstract

Preview control is investigated for active suspension systems. Two preview concepts are used: (1) look-ahead preview, where the information relating to roadway disturbances about to be encountered by the moving vehicle is assumed to be sensed, and (2) wheelbase preview, where knowledge of the front wheel states is used to improve performance at the rear of the vehicle. A method based on optimal control theory is presented to find the control laws for a half-car equipped with both fully active and slow-active systems under preview. The random road profile is assumed to be the output of a filtered white-noise process. Human perception of vibration is considered in the design of the active suspension systems. The design of the preview controller is reduced to the classical linear quadratic regulator of the original system and the previewed road inputs. Integral constraints are included in the performance index to achieve better body attitude control. The effect of preview control on vehicle performance characteristics in terms of ride comfort, suspension deflections and road-holding ability is investigated. The results show that the use of wheelbase preview along with look-ahead preview improves all aspects of the suspension performance.

Keywords

Active suspension, LQR, preview control, slow-active system, vehicle dynamics

Received 11 November 2009; accepted 4 January 2010

1. Introduction

Ride quality and handling performance of road vehicles are very much affected by the design of the vehicle suspension systems (VSS). Good ride quality requires a high damping setting at low frequencies to stifle bounce, roll and pitch, and lower damping settings at higher frequencies to avoid ride harshness. Improvement of handling performance, however, calls for the use of stiffer springs and dampers at all frequencies to provide good road-holding ability and reduce body attitude variation.

Because of the conflicting demands placed upon the VSS, and in order to meet the anticipated functional use of them, passive suspension has evolved to a high level of sophistication.

Unlike passive systems, which can only store or dissipate energy, active suspension can continuously change the energy flow to or from the system when required. Furthermore, the characteristics of an active suspension can adapt to instantaneous changes in driving conditions that can be detected by sensors. Therefore, active suspension systems may have the potential to improve the ride quality, road holding ability and safety of road vehicles through the control of suspension forces to satisfactory levels.

Over the past four decades, the subject of active suspension design has been intensively reviewed by Hedrick and Wormley (1975), Godall and Kortum (1983), Sharp and Crolla (1987), Masao Nagai (1993) and Hrovat (1997).

In fully active suspension systems, the dynamic suspension forces are generated using a high power, high speed device such as a hydraulic cylinder and electro-hydraulic valve combination. Better performance from using fully active systems (full bandwidth) are to be expected but with penalties. Such systems suffer from problems such as complexity, high cost and high power consumption. In addition, they need to be carefully designed to be reliable and fail-safe. However, a slow-active system can offer significant

[1] Department of Mechanical Engineering, King Saud University, Riyadh, Saudi Arabia
[2] Department of Mechanical Engineering, University of Nevada, Las Vegas, NV, USA

Corresponding Author:
M M ElMadany, Department of Mechanical Engineering, King Saud University, Riyadh, Saudi Arabia
Email: mmadany@ksu.edu.sa

improvements in the control of body resonances. This type of system offers advantages over full bandwidth active systems in the form of reduced power consumption and lower capital cost, and they have been preferred for production (Sharp and Hassan, 1987). Nevertheless, an important factor limiting the performance of active suspension is the lack of information on the oncoming road disturbances. More performance improvements can be achieved when the input from road irregularities can be measured in front of the vehicle and this information is utilized by the controller to prepare the system for the oncoming road input. This is called look-ahead preview and, in this case, the required control force can be synchronized in a much more efficient way.

There are two preview concepts. The first one uses "look-ahead sensors" to obtain the preview information. In this case, preview is available to control both the front and rear suspension. The preview sensor is assumed to be contactless and measures the variation in length of a reflected light, ultrasound or radar beam. The sensor is generally attached to the body on the front bumper to measure relative displacement between the car body and the road (Thompson et al., 1980; Yoshimura and Ananthanarayana, 1991; Hac, 1992; Huisman et al., 1993; Senthil and Narayanan, 1996; Mehra et al., 1997; Matsushita et al., 1997; Karlsson et al., 2001; ElMadany et al., 2003).

In the second concept (wheelbase preview), the road surface at the rear wheels is assumed to be the same as at the front wheels except for a time delay. So, if the road surface which contacts the front wheels can be determined, the preview is available and is used to improve performance at the rear wheels. The amount of preview is determined by the vehicle speed and its wheelbase (Abdel-Hady and Crolla, 1989; Pilbeam and Sharp, 1993; Sharp and Pilbeam, 1993; Yu et al., 2000; Kim et al., 2002; Qarmoush, 2004).

The above mentioned publications have shown that the optimal preview control of active suspension substantially relaxes the trade-offs between the conflicting requirements of the suspension, and the vehicle performance can be improved substantially.

In this work, it is proposed to develop an analytical design procedure that would yield mechanisms to control effectively the vehicle body acceleration for ride comfort, dynamic tire deflections and body attitude for ride handling and suspension deflections for the purpose of packaging by means of active suspension with preview. The objectives include: (1) development of a half-car model, which is adequate for understanding the effect of road disturbances on the ride and handling characteristics of the vehicle; (2) deriving the optimal preview control laws of two types of active suspension; a fully active system (FA) with full state feedback, and a slow-active system (SA) incorporating an actuator of limited bandwidth. The integral control action and the human perception of vibration are included in both systems; and (3) investigating the possibilities of performance improvements using the two preview concepts; i.e., look-ahead and wheelbase preview, together with the half-car model.

2. System Model

2.1. Model of Vehicle Ride Dynamics

In this study, a four degrees of freedom (4-DOF) half-car pitch bounce model of the vehicle is used. A schematic representation of this model, equipped with slow-active suspension components, is shown in Figure 1. The model is formulated as a linear lumped parameter model, consisting of three discrete rigid bodies, namely: the vehicle body (sprung mass) and wheel-axle assemblies in front and rear of the vehicle with associated linkages (unsprung masses). The degrees of freedom are determined under the following assumptions: (1) the vehicle is traveling over an uneven road at a constant forward speed; (2) the vehicle body is allowed to translate in the vertical direction (bounce/heave) and to pitch; (3) each wheel-axle assembly (unsprung mass) is allowed to translate in the vertical direction; (4) each suspension system is represented by a point contact model and exerts only vertical concentrated forces on the vehicle body; (5) each tire stiffness is represented by a linear spring element; (6) the vehicle system is excited by disturbances arising from roadway unevenness; and (7) the actuators are acting between the sprung mass (car body) and the unsprung masses.

Under these assumptions, the vibratory motions of the vehicle may be described in terms of 4-DOF, namely: bouncing and pitching motions of the sprung mass, x and θ, and the bouncing motions of each unsprung mass, x_1 and x_2. The values of vehicle parameters are given in Table 1, together with the values of damper coefficients corresponding to the proposed wheel damping ratios, and the parameters of the low-pass-filters (LPF) used with the limited bandwidth actuators (LBA) of the slow-active systems.

2.2. Suspension Models

The following types of suspension are considered in the simulations:

1. Slow-active system incorporating an actuator of limited bandwidth in series with a passive spring, the combination being in parallel with a passive damper. The slow-active system belongs to the class of displacement control problems. The limited bandwidth nature of each actuator is represented in the vehicle model by including two similar second-order low-pass-filters (LPF) in series with a perfect actuator. The use of these two filters is expected to make the actuators more effective in controlling lower frequency body modes (Pilbeam and Sharp, 1993; Sharp and Pilbeam, 1993).
2. Full bandwidth ideal active system with full state feedback, in which the control inputs to the system are the

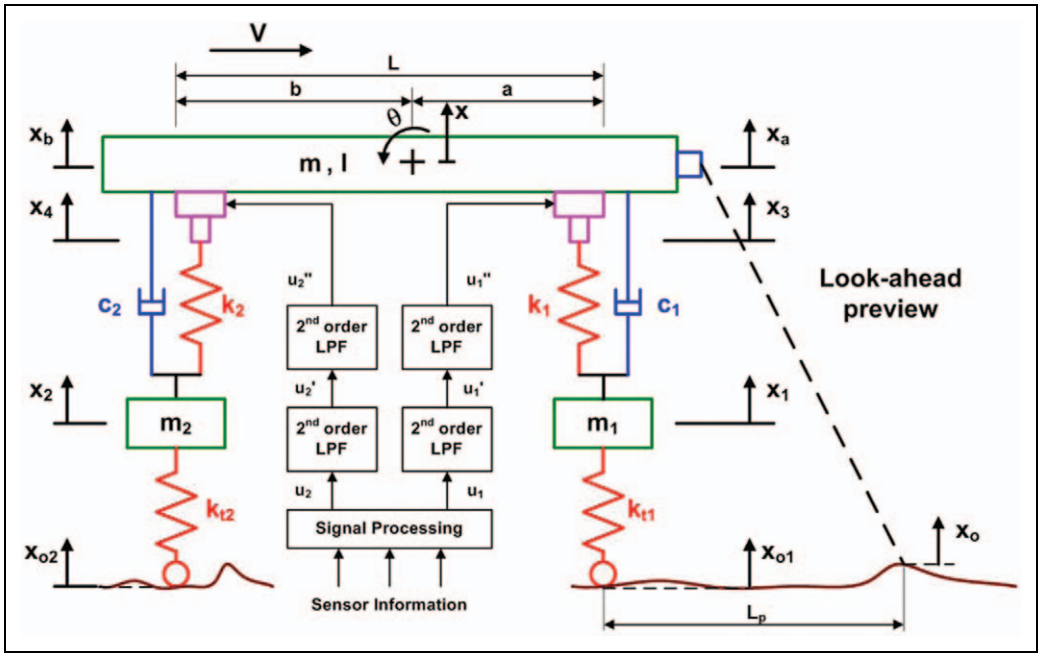

Figure 1. Half-car model equipped with slow-active suspension elements.

active suspension forces at the front and rear of the vehicle.

3. Passive system, in which the springs and dampers have linear characteristics.

2.3. Equations of Motion of Half-Car with Slow-Active Suspension

In this section, the equations governing the dynamic motion of the vehicle model equipped with a slow-active suspension system are described.

The general form of the equation for the second-order low-pass filters (LPF) is

$$\ddot{y} + 2\zeta\omega_c\dot{y} + \omega_c^2 y = \omega_c^2 x, \tag{1}$$

where x is the input signal, y is the output signal, $\omega_c$is the LPF cut-off frequency, and ζ is the LPF damping ratio.

The equation of vertical motion (heave) of the sprung mass is

$$m\ddot{x} = -F_a - F_b. \tag{2}$$

The equation of pitch motion of the sprung mass is

$$I\ddot{\theta} = -aF_a + bF_b. \tag{3}$$

The equations of vertical motion of front and rear unsprung masses are

$$m_1\ddot{x}_1 = F_a - F_{t1} \tag{4}$$

$$m_2\ddot{x}_2 = F_b - F_{t2} \tag{5}$$

where

Table 1. Values of vehicle parameters.

Symbol, unit	Value	Symbol, unit	Value
a, m	1.0978	b, m	1.4676
k_1, N/m	19960	k_2, N/m	22590
k_{t1}, N/m	155900	k_{t2}, N/m	155900
m, kg	505.1	I, kg.m^2	651
m_1, kg	28.58	m_2, kg	54.43
d, m	0.32		
c_1, N.s/m	438	c_2, N.s/m	582
ω_c, Hz	3	ζ	$1/\sqrt{2}$

$$F_a = k_1(x_3 - x_1) + c_1(\dot{x}_a - \dot{x}_1), \tag{6}$$

$$F_b = k_2(x_4 - x_2) + c_2(\dot{x}_b - \dot{x}_2), \tag{7}$$

$$F_{t1} = k_{t1}(x_1 - x_{o1}), \tag{8}$$

$$F_{t2} = k_{t2}(x_2 - x_{o2}), \tag{9}$$

where x_3 and x_4 are the front and rear LBA absolute output displacements, respectively, and x_a and x_b are the sprung mass displacement at front and rear tips given by

$$x_a = x + a\theta, \tag{10}$$

$$x_b = x - b\theta, \tag{11}$$

where θ is small to ensure linearity of the model.

Substituting F_a, F_b, F_{t1}, F_{t2}, x_a, x_b into equations 2, 3, 4 and 5 gives

$$\ddot{x} = \frac{1}{m}[(-ac_1 + bc_2)\dot{\theta} - (c_1 + c_2)\dot{x} + k_1x_1 + c_1\dot{x}_1 + k_2x_2 + \\ + c_2\dot{x}_2 - k_1x_3 - k_2x_4] \tag{12}$$

$$\ddot{\theta} = \frac{1}{I}[(-a^2c_1 - b^2c_2)\dot{\theta} + (-ac_1 + bc_2)\dot{x} + ak_1x_1 + ac_1\dot{x}_1 \\ - bk_2x_2 - bc_2\dot{x}_2 - ak_1x_3 + bk_2x_4]. \tag{13}$$

$$\ddot{x}_1 = \frac{1}{m_1}[ac_1\dot{\theta} + c_1\dot{x} - (k_1 + k_{t1})x_1 - c_1\dot{x}_1 + k_1x_3 + k_{t1}x_{o1}]. \tag{14}$$

$$\ddot{x}_2 = \frac{1}{m_2}[-bc_2\dot{\theta} + c_2\dot{x} - (k_2 + k_{t2})x_2 - c_2\dot{x}_2 \\ + k_2x_4 + k_{t2}x_{o2}]. \tag{15}$$

For the system in hand, the second-order LPF equations are

$$\ddot{u}_i' + 2\zeta\omega_c\dot{u}_i' + \omega_c^2u_i' = \omega_c^2u_i, \quad i = 1 \text{ and } 2 \tag{16}$$

$$\ddot{u}_i'' + 2\zeta\omega_c\dot{u}_i'' + \omega_c^2u_i'' = \omega_c^2u_i', \quad i = 1 \text{ and } 2 \tag{17}$$

where u_i' and u_i'' are the second- and fourth-order filtered control demand signals, respectively, while subscripts 1 and 2 define the front and rear properties, respectively, and

$$u_1'' = x_a - x_3, \tag{18}$$

$$u_2'' = x_b - x_4. \tag{19}$$

Substituting equations 10 and 11 into equations 18 and 19, respectively, gives

$$u_1'' = x + a\theta - x_3, \tag{20}$$

$$u_2'' = x - b\theta - x_4. \tag{21}$$

Separating x_3 and x_4 in equations 20 and 21 and taking the time derivatives twice, gives

$$\ddot{x}_3 = \ddot{x} + a\ddot{\theta} - \ddot{u}_1'', \tag{22}$$

$$\ddot{x}_4 = \ddot{x} - b\ddot{\theta} - \ddot{u}_2''. \tag{23}$$

Equation 17 may be rewritten as

$$\ddot{u}_i'' = \omega_c^2u_i' - 2\zeta\omega_c\dot{u}_i'' - \omega_c^2u_i'', \quad i = 1 \text{ and } 2. \tag{24}$$

Substituting equations 12, 13 and 24 into equations 22 and 23 and rearranging, gives

$$\ddot{x}_3 = a\omega_c^2\theta + (2a\zeta\omega_c - ac_1C_a + bc_2C_{ab})\dot{\theta} + \omega_c^2x \\ + (2\zeta\omega_c - c_1C_a - c_2C_{ab})\dot{x} + k_1C_ax_1 + c_1C_a\dot{x}_1 \\ + k_2C_{ab}x_2 + c_2C_{ab}\dot{x}_2 - (\omega_c^2 + k_1C_a)x_3 - 2\zeta\omega_c\dot{x}_3 \\ - k_2C_{ab}x_4 - \omega_c^2u_1', \tag{25}$$

$$\ddot{x}_4 = -b\omega_c^2\theta - (2b\zeta\omega_c + ac_1C_{ab} - bc_2C_b)\dot{\theta} + \omega_c^2x \\ + (2\zeta\omega_c - c_1C_{ab} - c_2C_b)\dot{x} + k_1C_{ab}x_1 + c_1C_{ab}\dot{x}_1 \\ + k_2C_bx_2 + c_2C_b\dot{x}_2 - k_1C_{ab}x_3 - (\omega_c^2 + k_2C_b)x_4 \\ - 2\zeta\omega_c\dot{x}_4 - \omega_c^2u_2', \tag{26}$$

where

$$C_a = \frac{1}{m} + \frac{a^2}{I}, C_{ab} = \frac{1}{m} - \frac{ab}{I}, C_b = \frac{1}{m} + \frac{b^2}{I}.$$

From equation 16, the following equations may be derived:

$$\ddot{u}_1' = -2\zeta\omega_c\dot{u}_1' - \omega_c^2u_1' + \omega_c^2u_1 \tag{27}$$

$$\ddot{u}_2' = -2\zeta\omega_c\dot{u}_2' - \omega_c^2u_2' + \omega_c^2u_2. \tag{28}$$

The governing equations of the system are then equations 12, 13, 14, 15, 25, 26, 27 and 28.

Introducing the following state, control input and disturbance vectors:

$$x_s = [\theta \quad \dot{\theta} \quad x \quad \dot{x} \quad x_1 \quad \dot{x}_1 \quad x_2 \quad \dot{x}_2 \quad x_3 \quad \dot{x}_3 \\ x_4 \quad \dot{x}_4 \quad u_1' \quad \dot{u}_1' \quad u_2' \quad \dot{u}_2']^{\mathrm{T}} \tag{29}$$

$$u = [u_1 \quad u_2]^{\mathrm{T}}, w = [x_{o1} \quad x_{o2}]^{\mathrm{T}}, \tag{30}$$

the equations of motion can be expressed in the following state form:

$$\dot{x}_s = A_sx_s + B_su + D_sw, \tag{31}$$

where A_s, B_s and D_s are matrices of dimensions $n\times n$, $n\times m$ and $n\times m$, where $n = 16$ and $m = 2$.

In order to control the body motion due to changes in payload, forces resulting from steering, braking, traction and aerodynamic forces, the system equations are augmented with the integral of the suspension working space, given by

$$\dot{p} = Sx_s, \tag{32}$$

where S is a 2×n matrix, defined by

$$S = \begin{bmatrix} a & 0 & 1 & 0 & -1 & 0 & 0 & 0 & 0 & 0 & 0 & 0 & 0 & 0 & 0 & 0 \\ -b & 0 & 1 & 0 & 0 & 0 & -1 & 0 & 0 & 0 & 0 & 0 & 0 & 0 & 0 & 0 \end{bmatrix}. \tag{33}$$

The augmented system equations then become

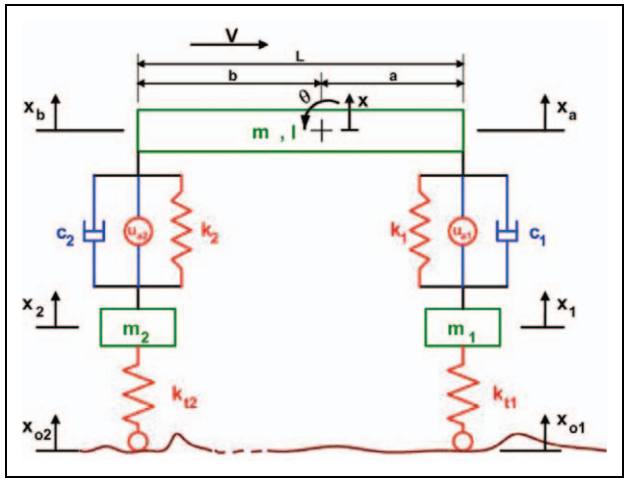

Figure 2. Half-car model with active and passive suspension components.

$$\dot{x}_{si} = A_{si}x_{si} + B_{si}u + D_{si}w, \tag{34}$$

where

$$x_{si} = [x_s^T \quad p^T]^T, \tag{35}$$

$$A_{si} = \begin{bmatrix} A_s & 0_{2\times2} \\ S & 0_{2\times2} \end{bmatrix}, \; B_{si} = \begin{bmatrix} B_s \\ 0_{2\times2} \end{bmatrix}, \; D_{si} = \begin{bmatrix} D_s \\ 0_{2\times2} \end{bmatrix}, \tag{36}$$

where $0_{2\times2}$ denotes a 2×2 matrix with zero elements.

2.4. Equations of Motion of Half-Car with Full Active Suspension

A schematic representation of a half-car model, equipped with both fully active and passive suspension components, is shown in Figure 2. In this study, for a fully active system, the springs and dampers are ignored while they are considered for passive system. The detailed derivation of the governing equations for the vehicle equipped with fully active suspension systems and passive suspension systems is given by Fayed (2007).

The equations of motion of the ideal fully active system can be expressed in the state-space representation as given below:

$$\dot{x}_f = A_f x_f + B_f u_a + D_f w, \tag{37}$$

where A_f, B_f and D_f are matrices of dimensions $n\times n$, $n\times m$ and $n\times m$, where $n = 8$ and $m = 2$.

2.5. Road Irregularities Model

In this study, two types of road irregularity are considered. The first one is the random road disturbance which represents the majority of irregularities encountered by vehicles in most of the motorways and highways. This type of road input is modeled as filtered white noise and investigated in the frequency domain. The other type is the deterministic road disturbance which may be represented by the regular step, sine or double slanted bumps. The effect of this type of disturbance on the performance of proposed vehicle models is studied in the time domain.

Table 2. Numerical values of road characteristics.

Road type	Road constant α (m^{-1})	Variance of road irregularities σ^2 (m^2)
Asphalt road	0.15	9×10^{-6}

2.5.1. Random Road Input. The input excitation to the vehicle model is assumed to be the apparent vertical roadway motion, caused by the vehicle's forward speed along a road having an irregular profile. Measurements of road profiles (Rotenberg, 1972) have indicated that road surface irregularities may be treated as a stationary Gaussian random process with zero mean and characterized by a power spectral density (PSD) of the form (Rotenberg, 1972; Muller et al., 1979),

$$\phi(\omega) = \frac{2\alpha v\sigma^2}{\pi}\frac{1}{\alpha^2v^2 + \omega^2}, \tag{38}$$

where σ^2 is the variance of road irregularities, α is a coefficient depending on the shape of the road irregularities, v is the vehicle's forward speed and ω is the road temporal frequency. The values of random road characteristics are listed in Table 2.

From the roughness representation, equation 38, the vehicle excitation model can be obtained in the time domain by using a shaping filter of the form

$$\dot{x}_o = -\alpha v x_o + \xi, \tag{39}$$

where ξ is a zero-mean white-noise process with

$$E[\xi(t)\,\xi(t-\tau)] = 2\alpha v\sigma^2\delta(\tau), \tag{40}$$

in which $\delta(.)$ denotes the Dirac delta function and E[.] is the expectation operator.

Since the vehicle is excited at front and rear wheels, the stochastic excitation process, $w(t)$, is characterized by the time delay

$$\tau = \frac{L}{v}, \tag{41}$$

where L is the distance between the front and rear wheels (wheelbase).

Thus, the road excitation model can be cast in the state variable form:

$$\dot{w} = A_w w + b_w\xi, \tag{42}$$

where w is the road excitation vector:

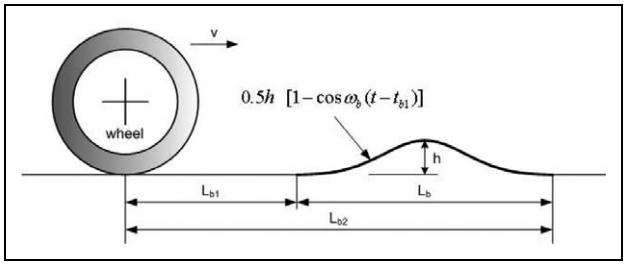

Figure 3. Schematic of the sine bump and vehicle wheel.

$$w = [x_{o1}\, x_{o2}]^{\mathrm{T}}, \tag{43}$$

$$A_w = -\alpha\, v\, I, \tag{44}$$

$$b_w = I, \tag{45}$$

ξ is the vector of time-delayed white-noise Gaussian disturbances with zero mean:

$$\xi = [\xi_1(t) \quad \xi_2(t)]^{\mathrm{T}}, \tag{46}$$

$$= [\xi_1(t) \quad \xi_1(t-\tau)]^{\mathrm{T}} \tag{47}$$

and where I is the 2×2 identity matrix.

2.5.2 Deterministic Road Input. The vehicle is assumed to travel over a single bump, similar to that in Hac (1992), described by

$$w(t) = \begin{cases} 0.5h\ [1-\cos\omega_b(t-t_{b1})] & for\ t \in [t_{b1}, t_{b2}] \\ 0 & otherwise \end{cases}. \tag{48}$$

where h is the bump height, t_b is the bump period, L_b is the bump length, v is the vehicle's forward speed, and ω_b is the bump frequency given by

$$\omega_b = \frac{2\pi}{t_b},\ t_b = \frac{L_b}{v}, \tag{49}$$

while t_{b1} is the time required for the wheel to hit (reach) the bump, which is also the preview time, and t_{b2} is the time required for the wheel to pass the bump. The times t_{b1} and t_{b2} are given by

$$t_{b1} = \frac{L_{b1}}{v},\ t_{b2} = \frac{L_{b2}}{v}, \tag{50}$$

where L_{b1} and L_{b2} are the distances between wheel and bump start and end, respectively, and are given by

$$L_{b2} = L_{b1} + L_b. \tag{51}$$

A schematic drawing describing the bump is shown in Figure 3. Also, the values of the variables relating to the bump are given in Table 3.

Table 3. Values of parameters relating to the sine bump.

Parameter	Unit	Definition	Value
h	m	bump height	0.05
L_{b1}	m	distance between wheel and start of bump	1-10
L_b	m	longitudinal length of bump	2.5

As shown in Table 3, the values of L_{b1} vary from 1 to 10 m to give different preview times ranging from about 0.05 to 0.5 s according to the vehicle's speed.

2.6. Human Perception of Vibration

The problem of isolating the driver from excessive vibration is a long-standing research topic in the vehicle industry. From practical experience and epidemiological studies, it is known that prolonged exposure to vibration during normal operation of high-speed vehicles (cars, buses, trucks, etc.), off-road vehicles and heavy machinery has adverse effects on the operator's health (ISO 7096-82, 1982; ISO 2631-1, 1997). For this reason, the human perception of vibration (HPA) must be considered when dealing with improvements and control of VSS.

The HPA is represented here by a shape filter that modifies the acceleration at the driver's location. Experimental studies of human perception of vibration have resulted in defining this shape filter in the vertical and longitudinal directions (ISO 2631-1, 1997). Thus, the HPA in any direction can be related to the induced measurable acceleration in that direction through the corresponding shape filter. The shape filter can be realized in terms of state variables by the following set of equations:

$$a_p = h_q^T q \tag{52}$$

and

$$\dot{q} = A_q q + g_q a_d, \tag{53}$$

$$= A_q q + g_q c_x^T x_s + g_q c_u^T u, \tag{54}$$

where a_p is the HPA and a_d is the induced measurable acceleration at the driver's position:

$$a_d = c_x^T x + c_u^T u. \tag{55}$$

Here c_x and c_u are weighting vectors resulting from the dynamic equations of motion. The sizes of c_x and c_u are n and m, respectively, where n = 16, m = 2, and, for a slow-active system, the elements of these vectors are given by

$$c_x(i,1) = A_s(2,i) + d \cdot A_s(4,i), \quad i = 1, 2, \quad \ldots, \ 16 \tag{56}$$

$$c_u(i,1) = B_s(2,i) + d \cdot B_s(4,i), \quad i = 1, 2 \tag{57}$$

where d is the distance from the driver's location to the sprung mass center of gravity.

In the vertical direction, the matrices A_q, g_q and h_q are given by (Muller et al., 1979)

$$A_q = \begin{bmatrix} 0 & 1 \\ -1200 & -50 \end{bmatrix}, g_q = \begin{bmatrix} 0 \\ 1 \end{bmatrix}, h_q = \begin{bmatrix} 500 \\ 50 \end{bmatrix}. \quad (58)$$

The vehicle system, equipped with a slow-active suspension system, with the integral states represented by equation 34, is augmented with additional states representing the road inputs, equation 42, and the HPA, equation 54. The resulting augmented system can be cast in the form

$$\dot{x}_{sa} = A_{sa}x_{sa} + B_{sa}u + D_{sa}\xi, \quad (59)$$

where

$$x_{sa} = [\, x_s^T \quad w^T \quad q^T \quad p^T \,]^T, \quad (60)$$

$$A_{sa} = \begin{bmatrix} A_s & D_s & 0_{16\times2} & 0_{16\times2} \\ 0_{2\times16} & A_w & 0_{2\times2} & 0_{2\times2} \\ g_q c_x^T & 0_{2\times2} & A_q & 0_{2\times2} \\ S & 0_{2\times2} & 0_{2\times2} & 0_{2\times2} \end{bmatrix},$$
$$B_{sa} = \begin{bmatrix} B_s \\ 0_{2\times2} \\ g_q c_u^T \\ 0_{2\times2} \end{bmatrix}, \; D_{sa} = \begin{bmatrix} 0_{16\times2} \\ b_w \\ 0_{2\times2} \\ 0_{2\times2} \end{bmatrix}, \quad (61)$$

where A_{sa}, B_{sa} and D_{sa} are matrices of dimension $n \times n$, $n \times m$ and $n \times m$, respectively, where $n = 22$ and $m = 2$. The 0 symbol denotes a matrix of all zero elements where the proper size is as indicated by its subscript. All other elements of these matrices are as previously defined for the corresponding equations.

The same augmentation process can be made for a vehicle system equipped with a fully active suspension. For more details, readers are referred to Fayed (2007).

2.7. Wheelbase Modeling for Preview Control

In this study, the correlation between front and rear wheel inputs is considered. This correlation introduces the principle of wheelbase preview. This type of preview can be understood if we realize the fact that the road disturbance at the rear wheel is the same as at the front wheel except for a time delay. Unlike the look-ahead preview, the benefits of wheelbase preview come without additional costs for sensors. The second-order Padé approximation is utilized to introduce this type of preview. The state-space description of the vehicle-road system is modified to include the correlation between the two road inputs.

The transfer function of the second-order Padé approximation is given in the frequency domain by

$$\frac{x_{o2}(s)}{x_{o1}(s)} = e^{-\tau s} = \frac{a_o - a_1 s}{a_o + a_1 s} \quad (62)$$

Where τ is the time delay between the front and rear inputs, $\tau = \frac{L}{v}$, s is a Laplace operator, x_{o1} is the random road displacement input at the front wheel, x_{o2} is the random road displacement input at the rear wheel, L is the wheelbase length, and a_o and a_1 are constant coefficients given below.

The state-space representation of equation 62 is given by

$$\dot{\eta}(t) = A_\eta \eta(t) + B_\eta \xi_f(t), \quad (63)$$

with output

$$\xi_r(t) = C_\eta \eta(t) + \xi_f(t), \quad (64)$$

where η is an additional state vector of order two, and A_η, B_η, C_η are constant matrices:

$$\eta = \begin{bmatrix} \eta_2 \\ \eta_1 \end{bmatrix}, A_\eta = \begin{bmatrix} 0 & 1 \\ -a_o & -a_1 \end{bmatrix}, B_\eta = \begin{bmatrix} -2a_1 \\ 6a_o \end{bmatrix}, C_\eta = [\, 1 \quad 0 \,], \quad (65)$$

where ξ_f is the road white-noise excitation encountered by the front wheel and ξ_r is the road white-noise excitation encountered by the rear wheel.

As reported by Athans and Falb (1966), the constants for the second-order Padé approximation (N = 2) are $a_o = 12/\tau^2$ and $a_1 = 6/\tau$.

Equation 3 may be extended as

$$\dot{w} = A_w w + b_{w1}\xi_f + b_{w2}\xi_r \quad (66)$$

where b_{w1}, b_{w2} are sub-matrices of b_w.

Substituting equation 64 into equation 66, gives

$$\dot{w} = A_w w + b_{w1}\xi_f + b_{w2}C_\eta \eta + b_{w2}\xi_f \quad (67)$$

or

$$\dot{w} = A_w w + b_{w2}C_\eta \eta + (b_{w1} + b_{w2})\xi_f. \quad (68)$$

With the last substitution, the rear disturbance is eliminated from equation 66, and hence the problem can be treated as a single input problem, the same way as in the uncorrelated case.

For the original VSS augmented with two road inputs, the HPA and the integral constraint, the governing equation 59 can be expanded to

$$\dot{x}_{sa} = A_{sa}x_{sa} + B_{sa}u + D_F\xi_f + D_R\xi_r \quad (69)$$

where D_F and D_R are sub-matrices of D_{sa} defined by its first and second columns, respectively.

Substituting ξ_r from equation 64 and rearranging, we obtain

$$\dot{x}_{sa} = A_{sa}x_{sa} + B_{sa}u + (D_F + D_R)\xi_f + D_R C_\eta \eta. \quad (70)$$

Combining equations 63 and 70 gives

$$\dot{x}_{sc} = A_{sc}x_{sc} + B_{sc}u + D_{sc}\xi_f \tag{71}$$

where

$$x_{sc} = \begin{bmatrix} x_{sa} \\ \eta \end{bmatrix},\ A_{sc} = \begin{bmatrix} A_{sa} & D_R C_\eta \\ 0_{2\times 22} & A_\eta \end{bmatrix},$$
$$B_{sc} = \begin{bmatrix} B_{sa} \\ 0_{2\times 2} \end{bmatrix},\ D_{sc} = \begin{bmatrix} D_F + D_R \\ B_\eta \end{bmatrix}, \tag{72}$$

where A_{sc}, B_{sc} and D_{sc} are matrices of dimension n × n, n × m and n × m, respectively, where n = 24 and m = 2. The 0 symbol denotes a matrix of all zero elements where the proper size is as indicated by its subscript.

3. Synthesis of the Controller

Due to the complexity of the system, the synthesis of the control law is based on linear-quadratic (LQ) theory. In this approach, a control law is obtained that minimizes a given performance index that trades off a number of performance objectives. This optimal control law requires full state feedback.

3.1. Performance Index

The performance index is written as a weighted sum of mean square values of output performance variables including HPA, suspension deflections, tire deflections, integral constraints and control effort:

$$J = \lim_{0\to\infty} \frac{1}{2T}\int_0^T [\rho_1 a_d^2 + \rho_2 \sum_{j=1}^{2} \Delta_{tj}^2 + \rho_3 \sum_{j=1}^{2} \Delta_{sj}^2 + \rho_4 \sum_{j=1}^{2} p_j^2 + \rho_R \sum_{j=1}^{2} u_j^2]dt \tag{73}$$

or

$$J = E\left[\rho_1 a_d^2 + \rho_2 \sum_{j=1}^{2} \Delta_{tj}^2 + \rho_3 \sum_{j=1}^{2} \Delta_{sj}^2 + \rho_4 \sum_{j=1}^{2} p_j^2 + \rho_R \sum_{j=1}^{2} u_j^2\right] \tag{74}$$

where E[.] denotes expected values or variances, a_d is the acceleration at the driver's position, Δ_{tj} are tire deflections, Δ_{sj} are suspension deflections and p_j are the suspension deflection integrals. The variables ρ_1, ρ_2, ρ_3, ρ_4, ρ_R are weighting factors which reflect the designer's preferences. By changing these weighting factors, various control laws can be derived which place different emphases on individual aspects of performance. The summations of Δ_{tj} and Δ_{sj} are given by

$$\sum_{j=1}^{2} \Delta_{tj}^2 = (x_1 - x_{o1})^2 + (x_2 - x_{o2})^2 \tag{75}$$

$$\sum_{j=1}^{2} \Delta_{sj}^2 = (x_a - x_1)^2 + (x_b - x_2)^2. \tag{76}$$

The performance index, equation 74, after simple algebraic manipulation with the system's equations of motions, can be put in the following matrix format, which is more convenient:

$$J = \lim_{T\to\infty} \frac{1}{2T}\int_0^T [x^T Q\, x + u^T R\, u + 2x^T N\, u]dt. \tag{77}$$

The last performance index is a weighted sum of variances of state variables, x, and control inputs, u. The matrices Q, R and N are all constant weighting matrices extracted by the manipulation of equation 77 and the vehicle model equations of motion.

3.2. Optimal Preview Control

Consider the linear system described by equation 71, given that the matrix A_{sc} is asymptotically stable. Assume that w(t) is an unknown *a priori* input with zero mean and $w(\tau)$, $\tau \in [t, t+t_p]$ is given deterministically. Consider also the performance criterion given by equation 77 in which Q is a symmetric and nonnegative definite matrix, R is a positive definite matrix such that $Q_n = Q - NR^{-1}N^T$ is nonnegative definite. Then the problem of determining an input which minimizes the criterion of equation 77 is called an optimal preview control problem.

The control law which minimizes performance has feedback and feedforward gains and is given by (Hac, 1992; Elbeheiry, 1998; ElMadany et al., 2003)

$$u = -K_1 x_{sc} - K_2 r, \tag{78}$$

where K_1 is the feedback gain given by

$$K_1 = R^{-1}[N^T + B_{sc}^T P], \tag{79}$$

and K_2 is the feedforward gain given by

$$K_2 = R^{-1}B_{sc}^T. \tag{80}$$

Here, P is the symmetric positive definite solution of the algebraic Riccati equation:

$$P A_n + A_n^T P - P B_{sc} R^{-1} B_{sc}^T P + Q_n = 0, \tag{81}$$

with

$$A_n = A_{sc} - B_{sc}R^{-1}N^T. \tag{82}$$

If, in addition, the pair (A_{sc}, B_{sc}) is stabilizable and (A_{sc}, $Q^{1/2}$) is detectable, then the closed-loop system is asymptotically stable.

The vector r is given by

$$r(t) = \int_0^{t_p} e^{A_c^T \sigma} P D_{sc}\, w(t+\sigma)d\sigma \tag{83}$$

where $A_c = A_{sc} - B_{sc}\, R^{-1}(N^T + B_{sc}{}^T P)$ is the closed-loop matrix which is asymptotically stable.

The controller, equation 78, is composed of a feedback part, $-R^{-1}(N^T + B_{sc}{}^T P)\, x$, which is an often used optimal control strategy for active suspension without preview, and a preview controller, $-R^{-1}\, B_{sc}{}^T\, r$, which is a feedforward part, containing the information about the road input obtained from preview sensors. The feedforward part utilizes preview to smooth out the vehicle's response.

The closed-loop system is described by

$$\dot{x}_{sc} = A_{sc}x_{sc} + B_{sc}R^{-1}B_{sc}^T r + D_{sc}\xi_f. \tag{84}$$

3.3. Power Spectral Density Analysis

The frequency domain transfer function matrix can be obtained by taking Fourier transforms of both sides of equation 84. This gives

$$x_{sc}(i\omega) = (i\omega I - A_{sc})^{-1}\Big[-B_{sc}R^{-1}B_{sc}^T \int_0^{t_p} e^{A_c\sigma} P\, D_{sc}\, e^{i\omega\sigma} d\sigma + D_{sc}\Big]\xi_f\,(i\omega) \tag{85}$$

where $x_{sc}(i\omega)$ and $\xi_f(i\omega)$ are the Fourier transformations of $x_{sc}(t)$ and $\xi_f(t)$, respectively.

The power spectral density matrix for the system is given by

$$S_o(\omega) = \bar{H}\,\bar{D}\,S_Q\bar{D}^*\bar{H}^*, \tag{86}$$

where $\bar{H}$ is the transfer function matrix expressed as

$$\bar{H} = [i\omega I - A_{sc}]^{-1}, \tag{87}$$

$$\bar{D} = -B_{sc}R^{-1}B_{sc}^T \int_0^{t_p} e^{A_c\sigma} P\, D_{sc} e^{i\omega\sigma} d\sigma + D_{sc}, \tag{88}$$

and * denotes complex conjugate transpose and S_Q is the road excitation spectral density given by

$$S_Q = \frac{2\alpha\, v\sigma^2}{\pi}. \tag{89}$$

4. Results and Discussion

The passive suspension system is taken as a reference model. The comparison with other systems with different control schemes is based on fixing the damping ratios of wheel hop assemblies for all systems for a soft mode ($\zeta_w = 0.1$). This fixation of damping ratios is made to maintain fairness of comparison. Unless otherwise specified, all simulations in the frequency domain are made for a vehicle speed of 20 m/s. The eigenvalues and damping ratios of the passive system are listed in Table 4, while the values of the RMS of its performance characteristics are listed in Table 5.

Table 4. Eigenvalues, damping ratios and natural frequencies for the passive suspension system.

	Soft mode, $\zeta_w = 0.1$		
Mode	natural frequency ω_n, rad/s	damping ratio ζ	eigenvalue λ
Body heave	8.093	0.079	$-0.641 \pm 8.068i$
Body pitch	10.5	0.116	$-1.217 \pm 10.429i$
Front wheel hop	57.173	0.1	$-5.733 \pm 56.884i$
Rear wheel hop	78.338	0.1	$-7.838 \pm 77.945i$

Table 5. RMS values of performance criteria for the passive suspension system.

Performance Criterion	Soft mode $\zeta_w = 0.1$
Front Tire Deflection (FTD), m	0.00125
Rear Tire Deflection (RTD), m	0.00143
Front Suspension Deflection (FSD), m	0.00402
Rear Suspension Deflection (RSD), m	0.00351
Human Perceived Acceleration (HPA), g's	0.02362

Beside the passive suspension system, the following types of suspension, all with full state feedback, are considered in the simulations:

- slow-active with integral control terms (SA+IC);
- slow-active with integral control terms and wheelbase preview (SA+IC+Cr);
- slow-active with integral control terms and both wheelbase and look-ahead preview actions (SA+IC+Cr+LA);
- ideal fully active with integral control terms (FA+IC);
- ideal fully active with integral control terms and wheelbase preview (FA+IC+Cr);
- ideal fully active with integral control terms and both wheelbase and look-ahead preview actions (FA+IC+Cr+LA).

The numerical values of the weighting factors in the performance index used in the simulation of an ideal fully active system and slow-active system are given in Table 6. Note that the weighting factor, ρ_1, is not applicable for fully active systems. This is because the spring rates and damping coefficients for fully active systems are set to zero and hence the car body acceleration is directly proportional to the control forces.

4.1. Response to Random Road Disturbances

The vehicle model equipped with different suspension systems has been simulated when traveling with a constant speed of 20 m/s on a randomly profiled road. The response

Table 6. The numerical values of weighting factors for fully active andslow-active systems.

Weighting factor	ρ_1	ρ_2	ρ_3	ρ_4	ρ_R
FA + IC	—	7.00×10^4	6.00×10^4	1.00×10^6	1.30×10^{-4}
SA + IC	7.50×10^{-3}	4.15×10^3	75.00	1.00×10^3	1.50

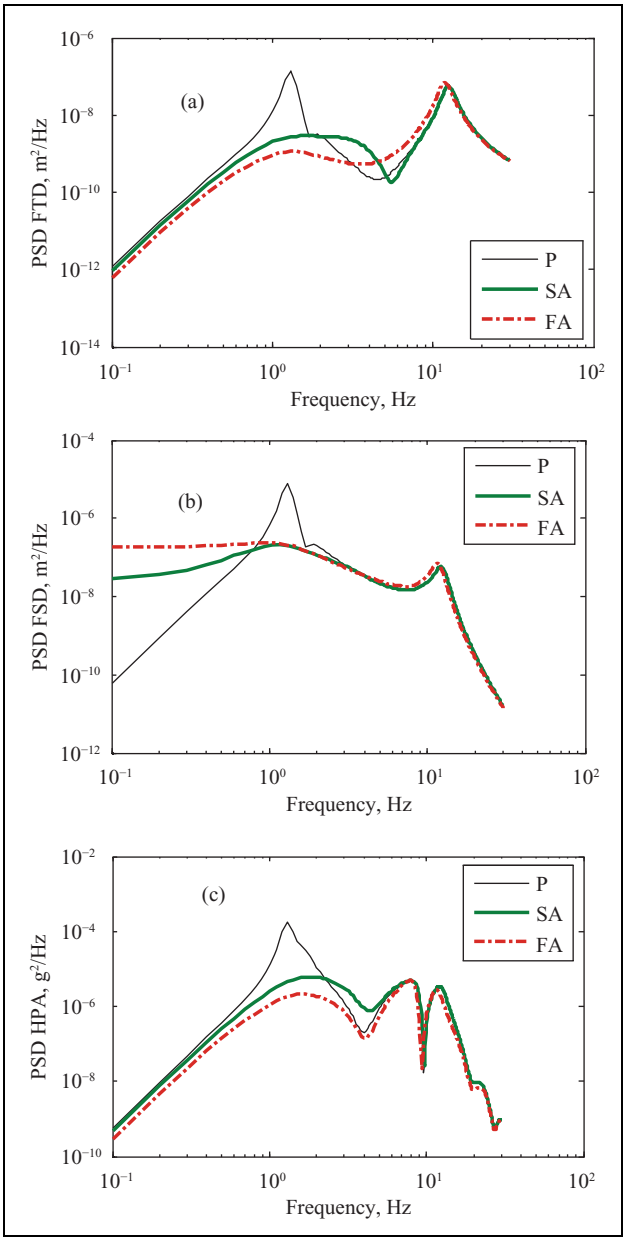

Figure 4. Response PSD for passive and active suspensions: (a) front tire deflection; (b) front suspension deflection; (c) human perceived acceleration.

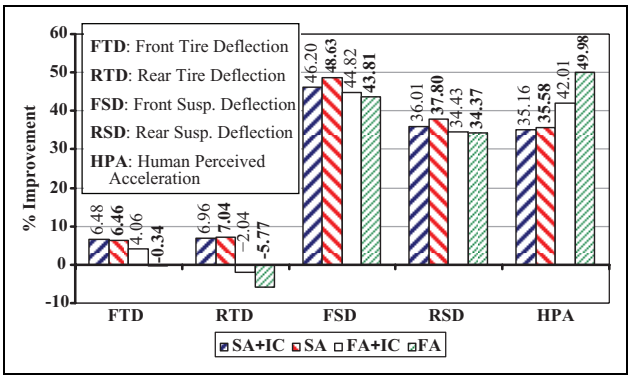

Figure 5. Percentage improvements in the RMS values of active systems w.r.t. the passive system.

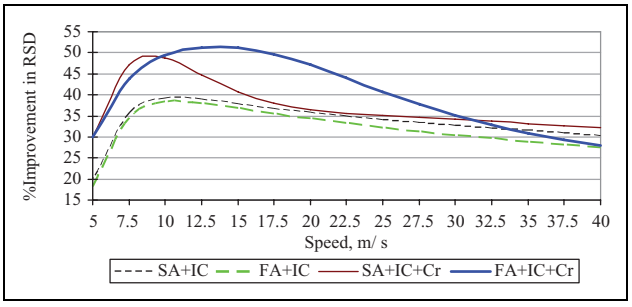

Figure 6. Percentage improvements in the RMS value of rear suspension deflection for active systems with and without wheelbase preview at different vehicle speeds.

spectra of a selected set of vehicle variables for the actively controlled and passive suspensions for soft mode are shown in Figure 4. The response spectra of the front tire deflection variation are shown in Figure 4(a). In the frequency range from 0.1 Hz to the wheel-hop frequency, a trade-off of attenuation and amplification is shown in the figure for the active suspension in comparison with the passive one. The slow-active system shows attenuation of the amplitude spectra in the frequency range of 0.6 to 2 Hz. The amplitude spectrum of the slow-active system would follow its passive system counterpart above 6 Hz. Therefore, it is clear that the passive spring that is connected in series with the actuator will dominate the tire deflection around the wheel-hop frequency. On the other hand, the fully active suspension amplifies the response above 3 Hz.

The power spectra of the suspension deflection at the front end are shown in Figure 4(b). Compromising results are shown as active systems are used. Increased suspension travel at low frequencies is noticed, accompanied by decreased amplification around body resonance frequencies for the actively controlled vehicle, compared with the

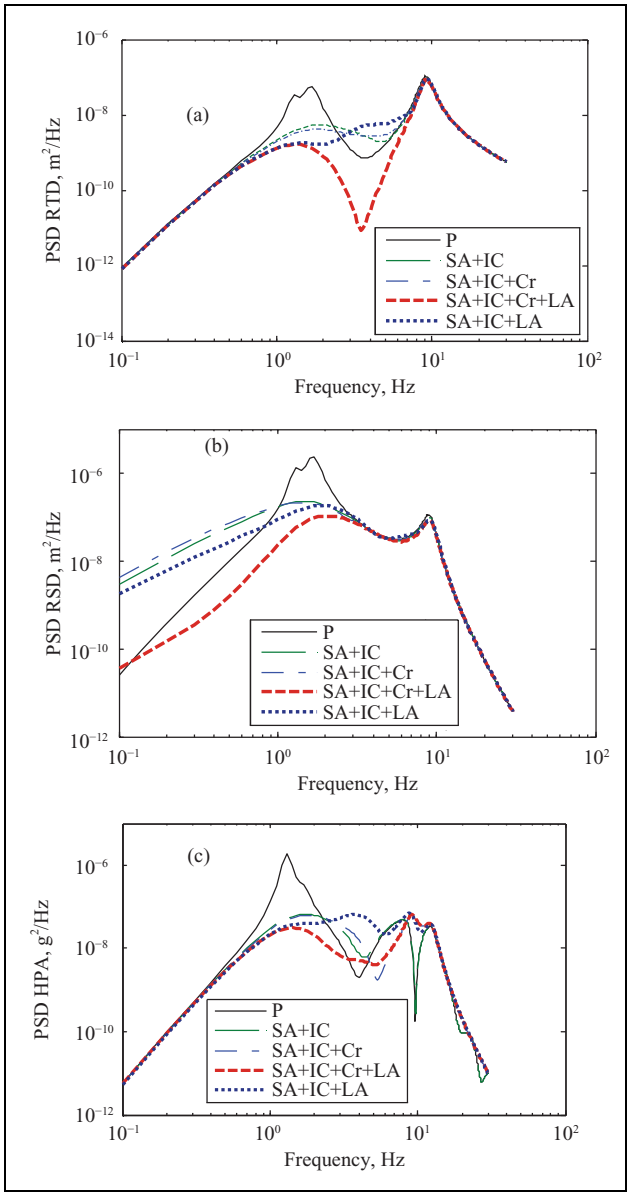

Figure 7. Response PSD for passive and slow-active suspensions with preview techniques, v = 20 m/s, t_p = 0.2 s: (a) rear tire deflection; (b) rear suspension deflection; (c) human perceived acceleration.

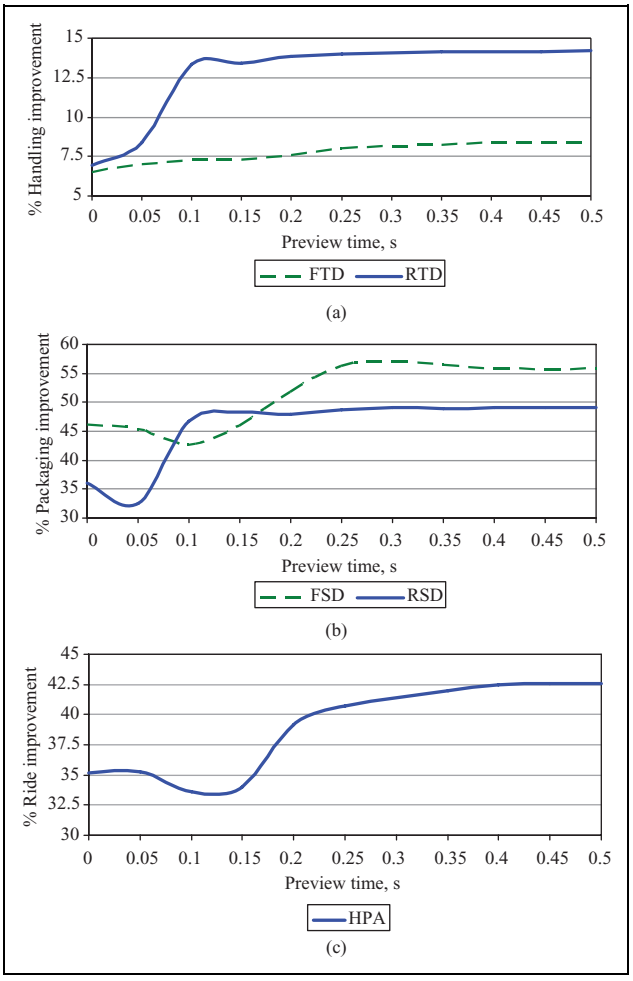

Figure 8. Percentage improvements in the RMS values achieved by a slow-active system with combined preview versus preview time, v = 20 m/s: (a) tire deflections; (b) suspension deflections; (c) human perceived acceleration.

passively suspended vehicle. The low frequency suspension travel for the controlled vehicles is the result of having different levels of inertial damping for the car body (sprung mass) and unsprung masses. It can be inferred from the figure that the slow-active system is as effective in damping body resonances as the fully active system. Regarding the acceleration spectra, the passive system shows two sharp peaks corresponding to the car body's natural frequencies, Figure 4(c). This is due to the presence of very low damping in these modes. However, these peaks are suppressed significantly and the response spectra are dominated by a wide band peak for the cases of using controlled suspensions. This is accomplished with negligible compromise of isolation at the wheel-hop frequency, compared with passive suspensions.

From examining the above presented results, it is clear that the fully active systems have only marginally greater performance potential than the slow-active one.

Figure 5 shows the percentage improvement in the RMS values of different performance criteria of fully active and slow-active suspension systems with respect to the passive system. These RMS values are calculated by integrating the PSD over the frequency range of 0.1 to 30 Hz. It is clear that the fully active suspension system has better improvements than all other systems in terms of ride quality, while the slow-active systems have more improvements in terms of handling and packaging.

The wheelbase preview control gives significant improvement for RMS values of performance for the rear wheel station without any additional cost for measurement and sensors. The individual performance improvement of

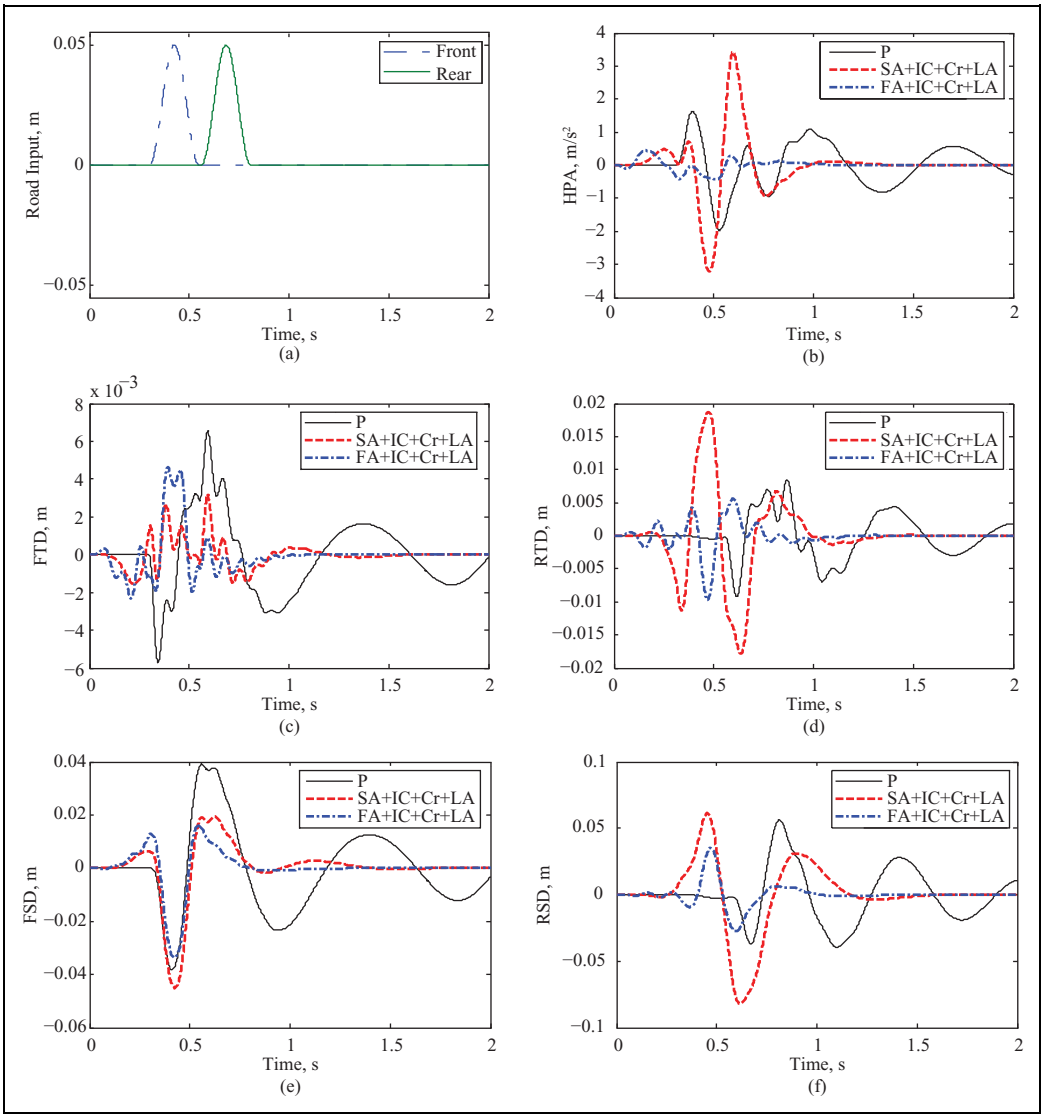

Figure 9. Response time histories of passive and different active systems with combined preview actions to sine bump, v = 10 m/s, t_p = 0.3 s: (a) road input; (b) human perceived acceleration; (c) front tire deflection; (d) rear tire deflection; (e) front suspension deflection; (f) rear suspension deflection.

this type of preview, in the case of slow-active suspensions, is limited to low speeds, up to 17 m/s as indicated by Figure 6. Beyond this speed, the improvements are less significant because the available preview time becomes shorter. This performance improvement is mainly in the rear suspension deflection. The optimum improvement in the RMS value of the rear suspension deflection, up to 49%, is achieved at speeds from 7 to 10 m/s.

Figure 7 shows that the look-ahead preview provides improvements in all vehicle performance criteria. In the case of the slow-active system with a preview time of 0.2 s, look-ahead preview control provides improvements in rear tire deflection, with respect to the non-preview case, in the frequency range of 0.7 to 3.1 Hz, Figure 7(a). In the case of rear suspension deflections, the look-ahead preview case gives remarkable improvements in the frequency range of 0.1 to 2 Hz, Figure 7(b). Regarding acceleration, the look-ahead preview case provides significant improvements in the frequency range of 0.9 to 4 Hz, as shown in Figure 7(c). From Figure 7 it is clear that the combination of both wheelbase and look-ahead preview gives the best performance over all other systems. It provides additional improvements in rear wheel station performance criteria and HPA relative to that achieved individually by both types of preview. Nevertheless, the application of this combined preview control scheme gives no further improvement in the front wheel station relative to individual wheelbase and look-ahead preview cases.

The percentage improvements in the RMS values of different vehicle characteristics achieved by using a

slow-active system with combined preview actions, both wheelbase and look-ahead, using different preview times are shown in Figure 8. Figure 8 indicates that the presence of combined preview actions in the vehicle slow-active suspension significantly reduces the RMS of all vehicle characteristics, compared to a slow-active system without these preview actions. It may be observed from the figure that there is an optimum preview time beyond which there is no further improvement. A reduction of more than 7% in the RMS of rear tire deflection, with respect to the non-preview case, is achieved with a preview time of 0.3 s, Figure 8(a), and a reduction of more than 10% in the RMS of suspension deflections is achieved with a preview time of 0.3 s, Figure 8(b). Also, a reduction of more than 7% in HPA is achieved with a preview time of 0.4 s, Figure 8(c).

4.2. Time Domain Analysis

A time domain simulation process was performed by using the fourth-order Runge-Kutta method in order to explore the performance features of the different control methods used in this study relative to each other and to those of the passive system. All the simulation results were obtained by considering the addition of a suspension integral constraint and the HPA. The vehicle's response to a deterministic road input in the form of a sine bump is examined. The mathematical description of this type of road input is given by equation 48.

The response time histories of both slow-active and fully active systems with combined preview actions are compared in Figure 9.

From examining Figure 9, it may be said that the active suspension systems, fully active and slow-active, exhibit smaller and better damped responses than passive suspension. The fully active suspension has the best results in terms of reduction of peak amplitudes and in quickly damping out oscillations. Using preview actions results in reduction of the suspension deflection, damping out quickly the tire deflection oscillations, but with a penalty in increasing the peaks of the human perception acceleration and rear wheel station characteristics for a slow-active system.

5. Conclusions

The following conclusions have been drawn:

1. A slow-active suspension system appears to have good performance comparable to that of a fully active system. It damps, very effectively, the body resonances. The controller based on wheelbase preview significantly improves the rear suspension performance of the actively controlled suspensions with a minor adverse effect on the ride comfort and handling. For a slow-active system, at a speed of 7.5 m/s, an improvement, over the uncorrelated case, of about 11% in rear suspension deflection is achieved along with a degradation in ride quality of about 3.5% and no effect on handling.
2. The use of combined preview actions, wheelbase and look-ahead, improves the performance of the actively controlled suspensions significantly. In the case of a slow-active system, an improvement of about 7% in ride comfort is obtained by using the combined preview control strategy over that without preview at a speed of 20 m/s and preview time of 0.4 s. It is strongly recommended to consider the use of correlation between front and rear wheel inputs in the design of the LQR of an active suspension system with look-ahead preview to get the optimum performance.

Acknowledgments:

The authors would like to thank the Research Center, College of Engineering, King Saud University for supporting this work under grant number 53/428. The assistance and encouragement of the Manufacturing Technology Transfer Project are also very much appreciated.

References

Abdel-Hady, M. B. A. and Crolla, D. A., 1989, "Theoretical analysis of active suspension performance using a four-wheel model," *Proceedings of the Institute of Mechanical Engineers* **203(D)**, 125–135.

Athans, M. and Falb, P. L., 1966, *Optimal Control: An Introduction to the Theory and its Applications*, McGraw-Hill.

ElMadany, M. M., Abduljabbar, Z., and Foda, M., 2003, "Optimal preview control of active suspensions with integral constraint," *Journal of Vibration and Control* **9**, 1377–1400.

Fayed, A. A., 2007, "Optimal preview control of active suspension systems," MSc thesis, King Saud University, Saudi Arabia.

Godall, R. M. and Kortum, W., 1983, "Active control in ground transportation – a review of the state-of-the-art and future potential," *Vehicle System Dynamics* **12**, 205–227.

Hac, A., 1992, "Optimal linear preview control of active suspension," *Vehicle System Dynamics* **21**, 167–195.

Hedrick, J. K. and Wormley, D. N., 1975, "Active suspension for ground transportation vehicle – a state-of-the-art review," *Mechanics of Transportation Systems, AMD* **15**, 21–40, (ASME).

Hrovat, V., 1997, "Survey of advanced suspension developments and related optimal control applications," *Automatica* **33(10)**, 1781–1817.

Huisman, R. G. M., Veldpaus, F. E., Voets, H. J. M., and Kok, J. J., 1993, "An optimal continuous time control strategy for active suspensions with preview," *Vehicle System Dynamics* **22**, 43–55.

ISO 7096-82, 1982, "Earth Moving Machinery-Operator Seat-Transmitted Vibration," First edition, *International Organization for Standardization*, Geneva.

ISO 2631-1, 1997, "Mechanical Vibration and Shock Evaluation of Human Exposure to Whole-Body Vibration," *International Organization for Standardization*, Geneva, pp. 1–31.

Karlesson, N., Dahleh, M., and Hrovat, D., 2001, "Nonlinear active suspension with preview," in *Proceedings, American Control Conference*, Arlington, VA, June 25-27, Vol. 4, pp. 2640–2645.

Kim, H.-J., Yang, H. S., and Park, Y., 2002, "Improving the vehicle performance with active suspension using road-sensing algorithm," *Computers & Structures* **80**, 1569–1577.

Louam, N., Wilson, D. A., and Sharp, R. S., 1992, "Optimization and performance enhancement of active suspensions for automobiles under preview of the road," *Vehicle System Dynamics* **21**, 39–63.

Matsushita, H., Dohta, S., and Noritsugu, T., 1997, "Preview control of pneumatic rear suspension using a disturbance observer," *Transactions, Japan Society of Mechanical Engineers*, Part C, **63(615)**, 3905–3910.

Mehra, R. K., Amin, J. N., Hedrick, K. J., Osorio, C., and Gopalasamy, S., 1997, "Active suspension using preview information and modal predictive control," in *Proceedings, IEEE International Conference on Control Applications*, Piscataway, NJ, USA, 97CH36055, pp. 860–865.

Muller, P. C., Popp, K., and Schiehlen, W. O., 1979, "Covariance analysis of nonlinear stochastic guideway-vehicle-systems," in *Proceedings, 6th IAVSD Symposium*, Technical University, Berlin, September, pp. 337–351.

Nagai, M., 1993, "Recent researches on active suspensions for ground vehicles," *JSME International Journal Series C* **36(2)**, 161–170.

Pilbeam, C. and Sharp, R. S., 1993, "On the preview control of limited bandwidth vehicle suspension," *Proceedings of the Institute of Mechanical Engineers* **207**, 185–193.

Qarmoush, A. O., 2004, "Ride performance of a slow-active suspension system based on a full vehicle model," MSc thesis, King Saud University, Saudi Arabia.

Rotenberg, R. W., 1972, "Vehicle suspension," Moskou: Mašinostrojenie (in Russian).

Senthil, S. and Narayanan, S., 1996, "Optimal preview control of a two-DOF vehicle model using stochastic optimal control theory," *Vehicle System Dynamics* **25**, 413–430.

Sharp, R. S. and Crolla, D. A., 1987, "Road vehicle suspension system design – a review," *Vehicle System Dynamics* **16**, 167–192.

Sharp, R. S. and Hassan, S. S., 1987, "Performance and design consideration for dissipative semi-active suspension systems for automobiles," *Proceedings, Institution of Mechanical Engineers* **Part D, Vol. 201(D2)**, 1–5.

Sharp, R. S. and Pilbeam, C., 1993, "On the ride comfort benefits available from road preview with slow-active car suspensions," in *Proceedings, 13th IAVSD Symposium*, pp. 437–448.

Thompson, A. G., Davis, B. R., and Pearce, C. E., 1980, "An optimal linear active suspension with finite preview," *Transactions, Society of Automotive Engineers* No. 800520.

Yoshimura, T. and Ananthanarayana, N., 1991, "Stochastic optimal control of vehicle suspension with preview on an irregular surface," *International Journal of System Science* **22**, 1599–1611.

Yu, F., Zhang, J.-W., and Crolla, D. A., 2000, "A study of a Kalman filter active vehicle suspension system using correlation of front and rear wheel road inputs," *Proceedings of the Institute of Mechanical Engineers* **214 Part D**, 493–502.